Geoscience Frontiers 5 (2014) 499–513

Contents lists available at ScienceDirect

China University of Geosciences (Beijing)

Geoscience Frontiers

journal homepage: www.elsevier.com/locate/gsf

Research paper

Geochronological, geochemical, and Nd-Hf isotopic studies of the Qinling Complex, central China: Implications for the evolutionary history of the North Qinling Orogenic Belt

Chunrong Diwu [a,*], Yong Sun [a], Yan Zhao [a], BingXiang Liu [b], Shaocong Lai [a]

[a] State Key Laboratory of Continental Dynamics, Department of Geology, Northwest University, Xi'an 710069, China
[b] Key Laboratory of Crust-Mantle Materials and Environments, School of Earth and Space Sciences, University of Science and Technology of China, Hefei 230026, China

ARTICLE INFO

Article history:
Received 2 December 2013
Received in revised form
26 March 2014
Accepted 2 April 2014
Available online 24 April 2014

Keywords:
Qinling Orogenic Belt
Qinling Complex
Rodinia
Partial melting
Zircon

ABSTRACT

The Qinling Complex of central China is thought to be the oldest rock unit and the inner core of the North Qinling Orogenic Belt (NQOB). Therefore, the Qinling Complex is the key to understanding the pre-Paleozoic evolution of the NQOB. The complex, which consists of metagraywackes and marbles, underwent regional amphibolite-facies metamorphism. In this study, we constrained the formation age of the Qinling Complex to the period between the late Mesoproterozoic and the early Neoproterozoic (ca. 1062–962 Ma), rather than the Paleoproterozoic as previously thought. The LA-ICP-MS data show two major metamorphic ages (ca. 499 and ca. 420–400 Ma) for the Qinling Complex. The former age is consistent with the peak metamorphic age of the high- and ultra-high pressure (HP-UHP) rocks in the Qinling Complex, indicating that both the HP-UHP rocks and their country rocks experienced intensive regional metamorphism during the Ordovician. The latter age may constrain the time of partial melting in the NQOB between the late Silurian and early Devonian. The Qinling Complex is mostly affiliated with subduction–accretion processes along an active continental margin, and should contain detritus deposited in a forearc basin.

The available data indicate that the NQOB was an independent micro-continent at least prior to the Neoproterozoic, and included a portion of the Grenville orogenic belt during the period of 1.2–0.8 Ga. The NQOB has experienced a unique geological history, which is obviously different from that of the North China Craton (NCC) and the Yangtze Craton during the Precambrian. The Neoproterozoic granitoids that intruded the Qinling Complex can be interpreted as the products of assembly of the supercontinent Rodinia. The NQOB was separated from Rodinia at ca. 830–740 Ma. Subsequently, the NQOB moved closer to the northern margin of the NCC, and the initial accretion or collision with the NCC occurred from the late Cambrian to the early Ordovician.

1. Introduction

The Qinling Orogenic Belt, which marks an irregular suture between the North China Craton (NCC) and the Yangtze Craton (Fig. 1a), is a major part of the east–west trending Central China Orogen of central China. The belt connects with the Qilian–Kunlun Orogenic Belt to the west and the Tongbai–Dabie Orogenic Belt to the east (Fig. 1b). The Qinling Orogenic Belt has experienced multiple stages of oceanic subduction, terrane accretion, and continental collision since the Proterozoic (Zhang et al., 2001; Dong et al., 2011b; Wu and Zheng, 2013); the belt has therefore been considered a composite orogenic belt.

Traditionally, the Qinling Orogenic Belt has been subdivided into south and north belts by the Shangdan suture zone (Fig. 1b) (Zhang et al., 2001). The southern Qinling Orogenic Belt (SQOB) consists of pre-Sinian basement overlain by Neoproterozoic to Triassic sedimentary rocks (Zhang et al., 2001). It is commonly

* Corresponding author. Tel.: +86 13109513339.
E-mail address: diwuchunrong@163.com (C. Diwu).

Peer-review under responsibility of China University of Geosciences (Beijing)

Production and hosting by Elsevier

1674-9871/$ – see front matter © 2014, China University of Geosciences (Beijing) and Peking University. Production and hosting by Elsevier B.V. All rights reserved.
http://dx.doi.org/10.1016/j.gsf.2014.04.001

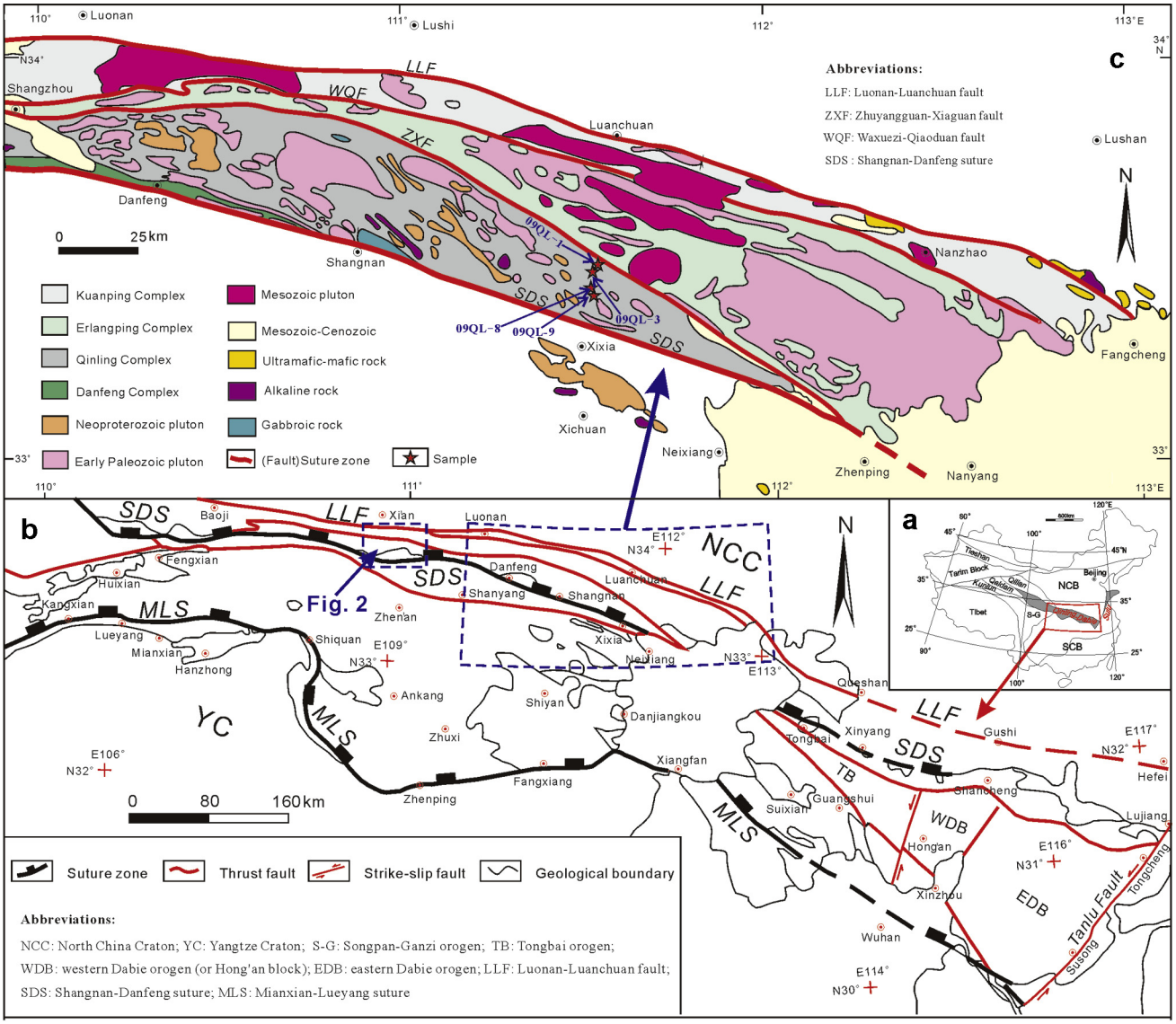

Figure 1. (a) Simplified geological map of China, (b) geological map of the Qinling–Dabie Orogenic Belt showing major tectonic units, and (c) geological map of the North Qinling Orogenic Belt (modified after Liu et al., 2013).

agreed that the SQOB was a passive continental margin on the northern margin of the Yangtze Craton (Zhang et al., 2001, 2002). However, the North Qinling Orogenic Belt (NQOB) displays different patterns of lithostratigraphy, metamorphism, basement deformation, and late Paleozoic cover sequences compared to that of the SQOB (Zhang et al., 2001), and the tectonic affinities of the NQOB remain controversial (Xu et al., 1997; Zhang et al., 2001; Diwu et al., 2010, 2012; Wu and Zheng, 2013). In addition, the tectonic evolution of the NQOB during the Precambrian remains uncertain.

The Qinling Complex is thought to be the oldest and innermost or core unit in the NQOB. Therefore, the complex is the key to understanding the generation and evolution of the Qinling Orogenic Belt prior to the Paleozoic. Although many have studied the complex, the nature of the protolith and the metamorphic ages of the complex remain poorly known. To address these problems, we present zircon U-Pb geochronology, major and trace element geochemistry, and Nd-Hf isotopic data on rocks of the Qinling Complex and intruded Neoproterozoic granites, with the aim to (1) constrain the timing of protolith formation and multiple metamorphic events; (2) unravel the tectonic affinities of the NQOB; and (3) combined with available data, determine the pre-Paleozoic tectonic evolution of the NQOB.

2. Geological setting

The NQOB is bounded to the north by the Luonan–Luanchuan–Fangcheng Fault and to the south by the Shangdan Fault (Fig. 1b). The belt is characterized by thick-skinned structures with dominantly southward-dipping imbricate thrusts and folds. From north to south, the main lithological units in the NQOB are the Kuanping Complex, the Erlangping Complex, the Qinling Complex, and the Danfeng Complex (Fig. 1c). These units are separated from one other by thrust faults or ductile shear zones (Zhang et al., 1996b, 2001).

2.1. Kuanping Complex

The Kuanping Complex is located in the northernmost part of the NQOB, and is separated from the Erlangping Complex in the

south by the 800-km-long east–west trending Zhuyangguan–Xiaguan Fault (Zhang et al., 2001). The Kuanping Complex is mainly exposed in the Beikuangping, Laoyu, Heihe, and Nanzhao areas.

Recent investigations indicate that the Kuanping Complex actually includes two tectonic units characterized by different lithologies, petrogenetic histories and ages (Diwu et al., 2010). The complex consists chiefly of metabasalts and metasedimentary rocks; the former are composed mainly of greenschists with intercalated amphibolites, and the latter of mica schists, quartzites, and marbles, the protoliths being wackes and carbonate rocks. LA-ICP-MS zircon U-Pb dating of a metabasalt from the Kuanping Complex yielded a weighted mean $^{207}Pb/^{206}Pb$ age of 943 Ma (Diwu et al., 2010), and the metabasalt has N-MORB type and T-MORB type geochemical characters (Zhang and Zhang, 1995; Diwu et al., 2010). However, the metasedimentary rocks of the Kuanping Complex were deposited during the early Phanerozoic, rather than during the Proterozoic (Diwu et al., 2010; Zhu et al., 2011).

2.2. Erlangping Complex

The Erlangping Complex, located in Henan Province, is separated from the Kuanping Group to the north by the Waxuezi–Qiaoduan Fault, and from the Qinling Complex to the south by the Zhuyangguan–Xiaguan Fault (Zhang et al., 2001). To the west, the equivalents of the Erlangping Complex are the Yunjiashan Group in the Luonan area and the Xieyuguan Group in the Meixian–Huxian area. The complex can be further divided into volcano–sedimentary sequences and an ophiolite unit (Sun et al., 1996). The Erlangping ophiolite unit is mainly composed of sparse ultramafic rocks, massive or pillow basalts, sheeted dikes and sills, cherts, and marbles. A large volume of volcanic and intrusive rocks that subsequently intruded the complex yields zircon U-Pb ages of ca. 443–480 Ma (Wang et al., 2012). Radiolarians in the cherts interlayered with the basalts imply that the basalts are of Ordovician to Silurian age (Wang et al., 1995; Sun et al., 1996). Trace element geochemistry shows that the mafic rocks of the ophiolite unit are mainly E-MORB and T-MORB metabasalts, suggesting that they were generated in a back-arc basin setting (Sun et al., 1996).

2.3. Danfeng Complex

The Danfeng Complex is located in the south of the NQOB along the shangdan suture. The complex is broadly exposed in the east of Danfeng County, in an east–west belt; it consists mainly of gabbros, basalts, andesites, small amounts of ultramafic rocks and minor sedimentary rocks. Isotopic data show that the complex formed at ca. 520–420 Ma (Dong et al., 2011a, and references therein). The complex is composed of N-MORBs and E-MORBs as well as arc-related volcanic rocks. Therefore, some researchers have suggested that the complex, which is located in the Shangdan suture zone, represents remnants of Shangdan oceanic crust, along with part of an island-arc succession (Dong et al., 2011a, b).

2.4. Qinling Complex

The Qinling Complex, which was traditionally named the 'Qinling Group', outcrops as several lenticular units in the NQOB, and extends for nearly 1000 km in an east–west direction. From west to east, the complex crops out mainly in the Taibai, Heihe–Laoyu–Fengyu, Danfeng–Shanxian–Xixia, and Tongbai areas (Zhang et al., 2001).

The Qinling Complex is a heterogeneous unit that can be divided into two distinct lithologic units. The upper unit consists of thick graphitic dolomite marbles and crystallized limestones, whose protoliths were carbonate rocks, whereas the lower unit comprises biotite plagioclase gneisses, amphibolites, garnet sillimanite biotite gneisses, and mica quartz schists, whose protoliths were dominantly metamorphosed argilloarenaceous and argillic rocks with minor volcanics. The relationship between the two lithologic units is debated: some researchers believe that both the marbles and gneisses belong to a continuous sedimentary sequence (Xiao et al., 1988; You et al., 1991), while others consider that the upper marbles are not constituents of the Qinling Complex, but rather belong to an allochthonous nappe emplaced during later tectonism (Zhang et al., 2001). Although the Qinling Complex has been studied intensively for over a decade, the formation age of the complex remains controversial. Published ages of the complex vary widely, ranging from early Proterozoic to Neoproterozoic (You et al., 1991; You et al., 1993; Zhang et al., 1996c; Shi et al., 2009; Wan et al., 2011a; Liu et al., 2013a), as do explanations of the obtained ages.

3. Sample description and petrography

Nine representative samples of the Qinling Complex were selected for this study. Of these, samples 08QL-1 and 08QL-6 were collected from the Fengyu area, Changan County, Shaanxi Province (Fig. 2), and samples 09QL-1, -2, -3, -4, -8, and -9 were collected from the Shewei area, Xixia County, Henan Province (Fig. 1c). The samples can be grouped into two lithological types: metasedimentary rocks in the Qinling Complex and Neoproterozoic granitic gneisses intruded into the Complex (Fig. 3). The first type includes samples 08QL-6, 09QL-1, and 09QL-3 (Fig. 3a–c). Sample 08QL-6, collected from the Weiziping area, is a garnet-bearing amphibole–biotite–monzonitic gneiss (Fig. 3c) displaying a gneissic structure and schistose granular texture; it is composed of plagioclase (~40%), microcline (~25%), quartz (~20%), mica (~10%), and amphibole (~5%). Samples 09QL-1 (09QL-2) (Fig. 3a) and 09QL-3 (09QL-4) (Fig. 3b), collected from the Shewei area, are a biotite–plagioclase gneiss and a mylonitized felsic gneiss, respectively. Samples 09QL-1 and 09QL-2 display blastoaleuritic textures and gneissic structures, and contain mica (~15%), plagioclase (~45%), and quartz (~40%). Samples 09QL-3 and 09QL-4 are characterized by strong ductile deformation, typical mylonite fabrics, and gneissic structures. Potassium feldspars (microcline) tend to be round or lens shaped, and form fragmented porphyroclasts with pressure shadows infilled by fine-grained recrystallized quartz aggregates. The porphyroclasts, which are reliable shear sense indicators, reveal left-lateral slip. The matrix is composed of a ribbon-like groundmass of mica, plagioclase, and quartz.

The second type is represented by samples 08QL-1, 09QL-8, and 09QL-9 (Fig. 3d–f). Sample 08QL-1, an amphibole biotite plagioclase gneiss (Fig. 3f) collected from the Weiziping area, displays gneissic and banded structure together with granoblastic texture, and is mainly composed of plagioclase (~45%), quartz (~40%), mica (~15%), and amphibole (~5%), with minor microcline (<2%) and titanite (~2%). Samples 09QL-8 (Fig. 3d) and 09QL-9 (Fig. 3e), collected from northern Tuqiaogang village, are garnet–biotite–monzonitic gneisses exhibiting gneissic structures with granular blastic textures, and consist of plagioclase (~40%), microcline (20–25%), quartz (20–25%), amphibole (~5%), and minor garnet (<2%).

4. Analytical methods

All analyses were performed at the State Key Laboratory of Continental Dynamics, Northwest University, Xi'an, China.

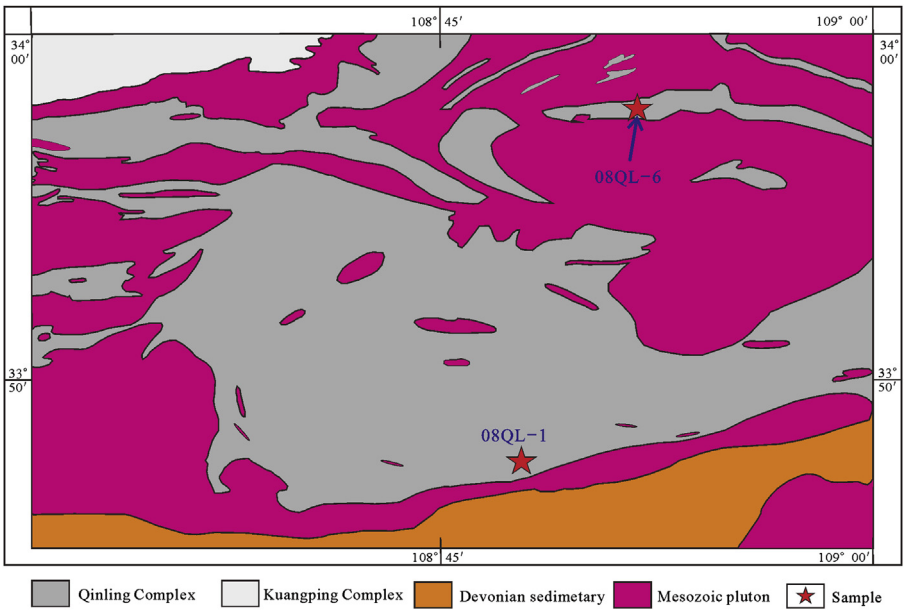

Figure 2. Simplified geological map of the Fengyu area.

4.1. Zircon collection and morphology

Zircons were separated by combined heavy liquid and magnetic separation techniques, and were then handpicked under a binocular microscope and mounted in epoxy resin. The mount was ground and polished until the zircon interiors were exposed. Zircons were photographed in reflected and transmitted light, and under cathodoluminescence (CL) imaging to reveal their internal structures. The CL imaging of the selected zircons was performed using a Quanta 400 FEG environmental scanning electron microscope equipped with an Oxford energy dispersive spectroscopy system and a Gatan CL3+ detector.

4.2. In situ zircon U-Pb dating and trace element analyses

In situ U-Pb dating and trace element analyses of zircons were performed on an Agilent 7500a ICP-MS instrument equipped with a 193-nm wavelength ArF-excimer laser (MicroLasTM Beam Delivery Systems, Lambda Physik AG, Germany). A fixed beam diameter of 30 μm and a laser repetition rate of 6 Hz were adopted throughout this study. Helium was used as the carrier gas to provide efficient aerosol delivery to the torch. The silicate glass standard NIST 610 was used to optimize the instrument to obtain maximum signal intensity (^{238}U signal intensity > 2000 cps/ppm at a beam diameter of 30 μm and a laser frequency of 6 Hz) and minimal oxide production (ThO/Th < 1%). The ion signal intensity ratios measured for ^{238}U and ^{232}Th (NIST SRM 610) (^{238}U and ^{232}Th ≈ 1) were used as indicators of complete vaporization (Günther and Hattendorf, 2005). The laser ablation strategy was to focus on a single laser spot on single zircons. Analyzed elements were collected in the time-resolved single-point per-peak mode. Dwell times were set to 10 ms for Th; 15 ms for U, Pb, and Ti; and 6 ms for other elements. The dual detector mode (pulse and analog counting) uses a short integration time. Here, ^{207}Pb/^{206}Pb, ^{206}Pb/^{238}U, ^{207}Pb/^{235}U, and ^{208}Pb/^{232}Th ratios were calculated using the software GLITTER 4.0 (Macquarie University), with the Harvard zircon 91500 used as an external reference (recommended ^{206}Pb/^{238}U age of 1065.4 ± 0.6 Ma) (Wiedenbeck et al., 2004) to correct for both instrumental mass bias and depth-dependent elemental and isotopic fractionation. Pooled ages were plotted and calculated using ISOPLOT/Excel version 3.6 (Ludwig, 2003). Concentrations of U, Th, Pb, and trace elements in zircons were calibrated using ^{29}Si as an internal standard and NIST SRM 610 as an external standard.

4.3. Lu-Hf isotopic analyses

Zircon Hf isotopic analyses were performed on a Nu Plasma HR MC-ICP-MS (Nu Instruments Ltd., UK) equipped with a GeoLas 2005 193-nm ArF-excimer laser-ablation system. Analyses were conducted using a spot size of 44 μm and He as a carrier gas. The laser repetition rate was 10 Hz, and the energy density applied was 15–20 J/cm^2. Raw count rates for ^{172}Yb, ^{173}Yb, ^{175}Lu, ^{176}(Hf + Yb + Lu), ^{177}Hf, ^{178}Hf, ^{179}Hf, and ^{180}Hf were collected simultaneously. The isobaric interference of ^{176}Lu on ^{176}Hf was corrected by measuring the intensity of an interference-free ^{175}Lu isotope and a recommended ^{176}Lu/^{175}Lu ratio of 0.02669 to calculate ^{176}Lu/^{177}Hf. Similarly, the interference of ^{176}Yb on ^{176}Hf was corrected by measuring an interference-free ^{172}Yb isotope and using a ^{176}Yb/^{172}Yb ratio of 0.5886 to calculate ^{176}Hf/^{177}Hf (Chu et al., 2002). Time-dependent drifts of Lu-Hf isotopic ratios were corrected using a linear interpolation according to variations of 91500 and GJ-1. To check data quality, 91500 and GJ-1 were reanalyzed as unknown samples. The obtained ^{176}Hf/^{177}Hf ratios were 0.282295 ± 0.000027 (n = 14, 2σ) for 91500 and 0.282734 ± 0.000015 (n = 16, 2σ) for GJ-1. These results are in good agreement with recommended ^{176}Hf/^{177}Hf ratios (0.2823075 ± 58, 2σ; 0.282015 ± 0.000019, 2σ) within 2σ (Wu et al., 2006).

Data processing was based on a decay constant for ^{176}Lu of 1.867 × 10^{-11} yr^{-1} (Albarède et al., 2006), and present-day chondritic ratios of ^{176}Hf/^{177}Hf = 0.282772 and ^{176}Lu/^{177}Hf = 0.0332 (BlichertToft and Albarede, 1997) for the calculation of ε_{Hf}. Single-stage model ages (t_{DM1}) were calculated by reference to depleted mantle with a present-day ^{176}Hf/^{177}Hf ratio of 0.28325 and an ^{176}Lu/^{177}Hf ratio of 0.0384 (Griffin et al., 2000). The two-stage model age (t_{DM2}) was calculated by projecting the initial ^{176}Hf/^{177}Hf of zircon back to the depleted mantle growth curve using a value of ^{176}Lu/^{177}Hf = 0.015 for average continental crust (Rudnick and Gao, 2003).

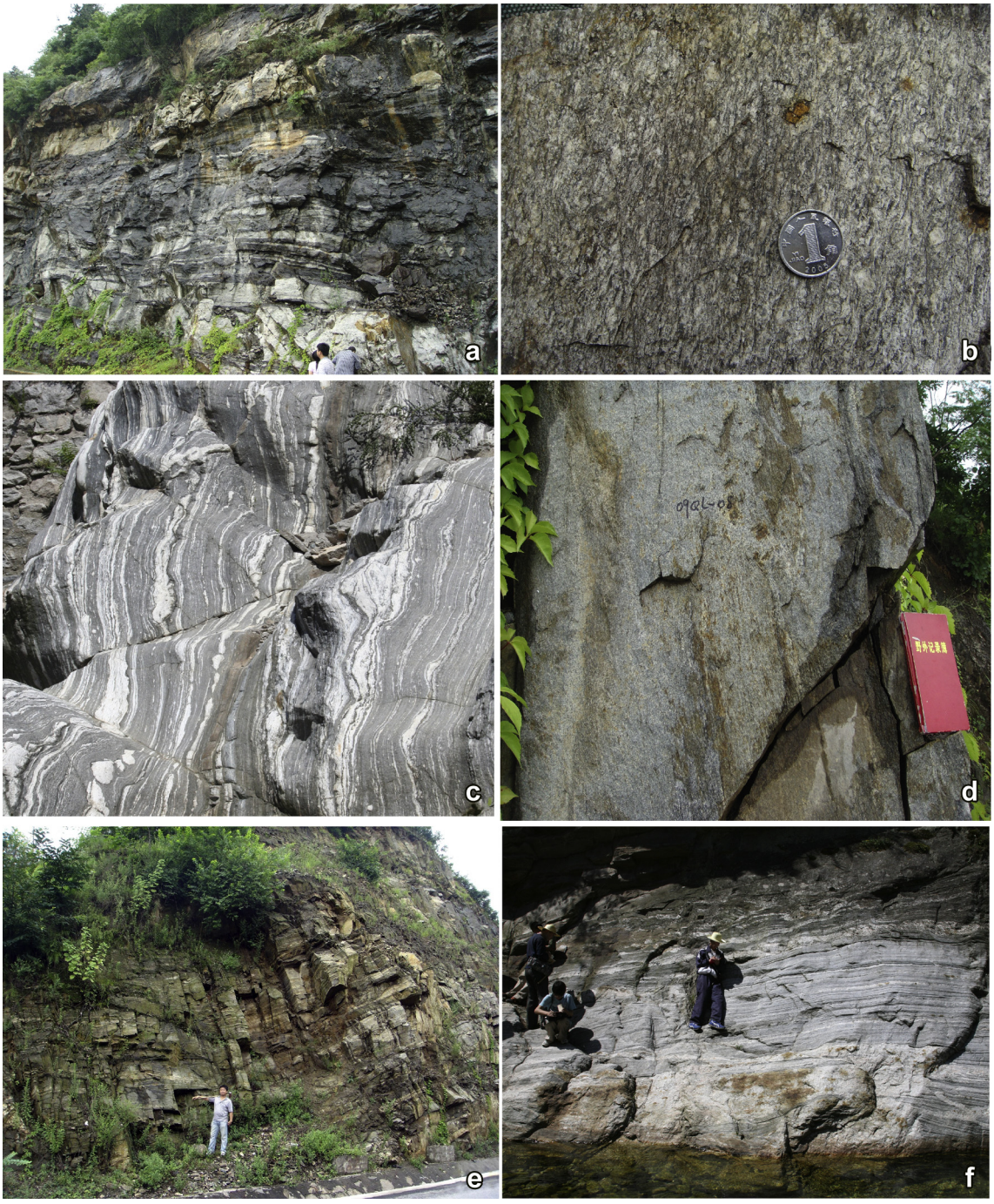

Figure 3. Selected field photographs of the Qinling Complex and related Neoproterozoic granitic gneisses. (a) Biotite–plagioclase gneiss in northern Shewei County (locality of sample 09QL-1). (b) NW–SE trending shear zone in the Shewei area dominated by mylonitized felsic gneiss (locality of sample 09QL-3); K-feldspars (microcline) tend to be lens shaped, and form fragmented porphyroclasts with pressure shadows; these porphyroclasts are reliable shear sense indicators, revealing left-lateral slip. (c) Biotite–monzonitic gneisses in the Weiziping area; the rocks are incorporated and folded within abundant anatectic veins (locality of sample 08QL-6). (d), (e) Neoproterozoic granitic gneisses in northern Xixia County (localities of samples 09QL-8 and 09QL-9, respectively). (f) Neoproterozoic granitic gneisses in the Weiziping area (locality of sample 08QL-1).

4.4. Major and trace element analyses of whole rock

Altered surfaces were carefully removed from all selected samples and the samples were washed and crushed to about 60 mesh in an alumina jaw crusher. Approximately 60 g of sample was powdered in a WC Mill (T1-100, CMT) to less than 200 mesh (75 μm) for whole-rock analyses.

Major element oxides were determined by XRF (Rigaku RIX 2100) using Li–borate glass disks. Analyses of international (USGS) rock standards BHVO-1 and AGV-1 indicate precisions and accuracies both better than 5%. Trace and rare earth elements were measured using an Agilent 7500a ICP-MS. Approximately 50 mg samples were dissolved in a sealed high-temperature and high-pressure bomb using equal parts of super-pure HF and HNO_3.

Analyses of USGS rock standards BHVO-1 and AGV-1 indicate that the analytical precision is mostly better than 5% (expressed in terms of the relative standard deviation).

4.5. Whole-rock Sm-Nd isotopic analyses

Whole-rock sample powders were decomposed in Teflon bombs using HNO_3–HF–$HClO_4$ mixed acid mixtures, and were loaded onto a column that contained AG50W-X8 resin (200–400 mesh) to separate rare earth element; subsequently, Nd isotopes were separated from the REEs using an Ln-spec ion exchange column. The Nd isotope analyses were performed on a Nu Plasma HR MC-ICP-MS (Nu Instruments Ltd., UK). During the period of analysis, the La Jolla reference material yielded a mean $^{143}Nd/^{144}Nd$ value of 0.511859 ± 6 (n = 10, 2s).

5. Results

The CL images of representative zircons are shown in Fig. 4, and the U-Pb data, Hf isotopic compositions, and Sm-Nd isotopic and major/trace element results are presented in Supplementary Tables 1–4, respectively.

5.1. Zircon U-Pb geochronology

Zircons in sample QL08-6 are commonly 100–200 μm in size and ellipsoidal in shape (Fig. 4a). The CL images revealed that most zircons are not zoned, which is typical of metamorphic zircons. A few zircons have cores surrounded by strongly luminescent rims, indicating that the metamorphic zircons underwent partial melting (Hoskin and Black, 2002; Brown, 2007; Wu et al., 2007). The zircon cores are weakly zoned, which provides evidence that the zircons are inherited magmatic zircons (Fig. 4a). We performed U-Pb analyses on eight cores. The oldest age was 2591 Ma, and the remaining seven zircons yielded an upper intercept age of 1036 ± 88 Ma (Fig. 5a). Analyses performed on 26 metamorphic rims and crystals gave $^{206}Pb/^{238}U$ ages of the dominant population of ca. 488–396 Ma, with a peak age at ca. 420 Ma (Fig. 5b).

Zircons in 09QL-1 are round or oval in shape, and commonly less than 100 μm in size (Fig. 4b). The round or oval grains are weakly luminescent, which is typical of metamorphic zircons, indicating that they experienced different degrees of solid-state recrystallization (Hoskin and Black, 2002; Brown, 2007; Wu et al., 2007). A few zircons exhibit core–rim structures and patched zoning in the core, suggesting they were modified by later metamorphism (Fig. 4b). Dating of 35 zircon grains gave four older ages of 1633, 1613, 1275, and 1056 Ma (#11, #53, #07, and #51, respectively); the other 31 samples yielded an upper intercept age of 1062 ± 170 Ma (Fig. 5c). The $^{206}Pb/^{238}U$ ages of metamorphic zircons varied from 426 to 363 Ma, with an obvious peak at ca. 405 Ma.

Zircons in sample 09QL-3 varied in size from 20 to 150 μm. In CL images, nearly half of the zircons showed core–rim structures (Fig. 4c). The cores exhibited clear oscillatory zoning, indicating that they are inherited magmatic zircons; their corresponding overgrowth rims showed comparatively weak luminescence, suggesting that they crystallized from a metamorphic melt (Hoskin and Black, 2002; Brown, 2007; Wu et al., 2007). The remaining zircons were black in CL images, which is typical of metamorphic zircons (Fig. 4c). Eighteen U-Pb analyses were performed on 18 cores, yielding ages of 1850–1163 Ma. Eleven younger magmatic cores yielded an upper intercept age of 1033 ± 41 Ma (Fig. 5e). Fifteen metamorphic zircons yielded a weighted mean $^{206}Pb/^{238}U$ age of 499 ± 7 Ma (MSWD = 1.2) (Fig. 5f); in addition, five metamorphic zircons gave ages of 461–406 Ma, representing the timing of anatexis in this sample.

Zircons in samples 08QL-1, 09QL-8, and 09QL-9 are short–long prismatic in shape. They exhibit oscillatory zoning with thin bright or dark rims, representing magmatic zircons that underwent different degrees of recrystallization (Hoskin and Black, 2002; Brown, 2007; Wu et al., 2007) (Fig. 4d–f). The magmatic cores from samples 08QL-1 and 09QL-8 are discordant, with upper intercept ages of 915 ± 43 Ma (MSWD = 5.1; n = 53) (Fig. 6a) and 960 ± 3 Ma (MSWD = 4.2; n = 27), respectively (Fig. 6b). Thirty-nine zircons were analyzed from sample 09QL-9, yielding an upper intercept age of 962 ± 16 Ma (MSWD = 3.2) (Fig. 6c) and a weighted mean $^{206}Pb/^{238}U$ age of 967 ± 15 Ma (Fig. 6d); the two ages are identical (within error). All upper intercept ages are interpreted as the times of intrusion of the protoliths of the three samples.

5.2. Zircon Lu-Hf isotopes

Twenty one Lu-Hf analyses were performed on 22 magmatic zircon grains from sample 09QL-8, yielding $^{176}Hf/^{177}Hf$ ratios of 0.281906–0.282337 and corresponding $\varepsilon_{Hf}(t)$ values of −10.0 to 5.0 at t = 960 Ma. Their two-stage Hf model ages vary from 2442 to 1501 Ma, with a mean age of 1938 Ma (Fig. 7a).

Magmatic zircons from sample 09QL-9 showed variable $^{176}Hf/^{177}Hf$ ratios ranging from 0.282192 to 0.282264, corresponding to $\varepsilon_{Hf}(t)$ values of −11.2 to 7.3 at t = 962 Ma. Their two-stage crustal model ages vary from 2670 to 1577 Ma, with a mean age of 1869 Ma (Fig. 7a).

Twenty-two Lu-Hf analyses were obtained from 22 metamorphic zircon grains from sample 08QL-6, exhibiting $^{176}Hf/^{177}Hf$ ratios of 0.281911–0.282895. Their $\varepsilon_{Hf}(t)$ values, calculated using their corresponding $^{206}Pb/^{238}U$ ages, varied from −21.7 to 13.7 (Fig. 7a), yielding two-stage Hf model ages of 1884–512 Ma.

5.3. Whole-rock Nd isotopes

The Sm-Nd isotopes of eight whole-rock samples from the Qinling Complex and the Neoproterozoic granitic gneisses are shown in Fig. 7b. In this diagram, the variations in initial $^{143}Nd/^{144}Nd$ ratios are expressed as $\varepsilon_{Nd}(t)$ values. Except for sample 08QL-6, which has a positive $\varepsilon_{Nd}(t)$ value, the other four samples yield negative $\varepsilon_{Nd}(t)$ values (−6.6 to −3.86), with two-stage Nd model ages of 2041–1818 Ma.

5.4. Major and trace elements

The SiO_2 content of the metasedimentary rocks of the Qinling Complex varies from 65.52 to 71.90 wt.%; the Al_2O_3 content ranges from 15.1 to 16.85 wt.%; and the Na_2O and K_2O contents range from 1.7 to 3.78 wt.% and 1.7 to 4.39 wt.%, respectively. On an SiO_2/Al_2O_3 and Na_2O/K_2O classification diagram (Pettijohn et al., 1987) (Fig. 8a), most samples are classified as graywackes and litharenites, indicative of their low maturities. They have low CaO contents (0.62–2.98 wt.%). Samples 08QL-6, 09QL-1, and 09QL-2 have elevated Fe_2O_3 contents (5.46–6.88 wt.%), reflecting the presence of Fe-bearing minerals such as amphibole and mica. The REE patterns of the metasedimentary rocks are LREE enriched ($(La/Yb)_N$ = 9.22–36.75) with negative Eu anomalies (Eu/Eu* values of 0.49–0.80) (Fig. 9a). On a PM-normalized trace element diagram, the samples show multi-element patterns similar to those of upper continental crust (Rudnick and Gao, 2003); strong negative Nb-Ta, P, and Ti anomalies; and slight Zr-Hf depletion (Fig. 9b).

The Neoproterozoic granitic gneisses have felsic compositions, with silica contents of 65.53–73.89 wt.%. The rocks belong to the high-K calc-alkaline series (Fig. 10a) and are peraluminous, with mol. $Al_2O_3/(K_2O + Na_2O + CaO)$ (A/CNK) ratios of 1.07–1.17 (Fig. 10b). They have relatively low MgO contents (0.36–1.70 wt.%)

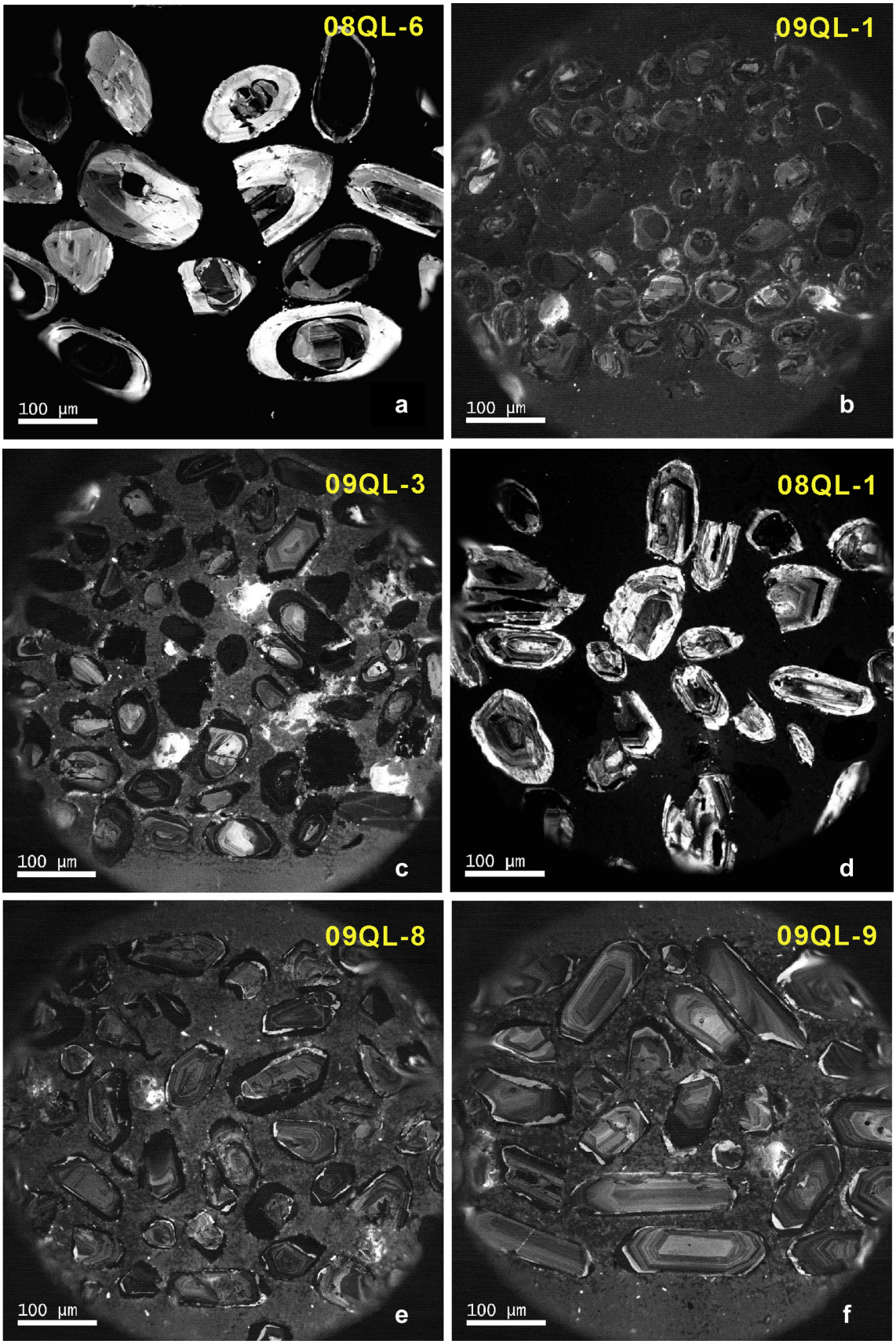

Figure 4. Cathodoluminescence (CL) images of zircons from the Qinling complex and from Neoproterozoic granitic gneisses.

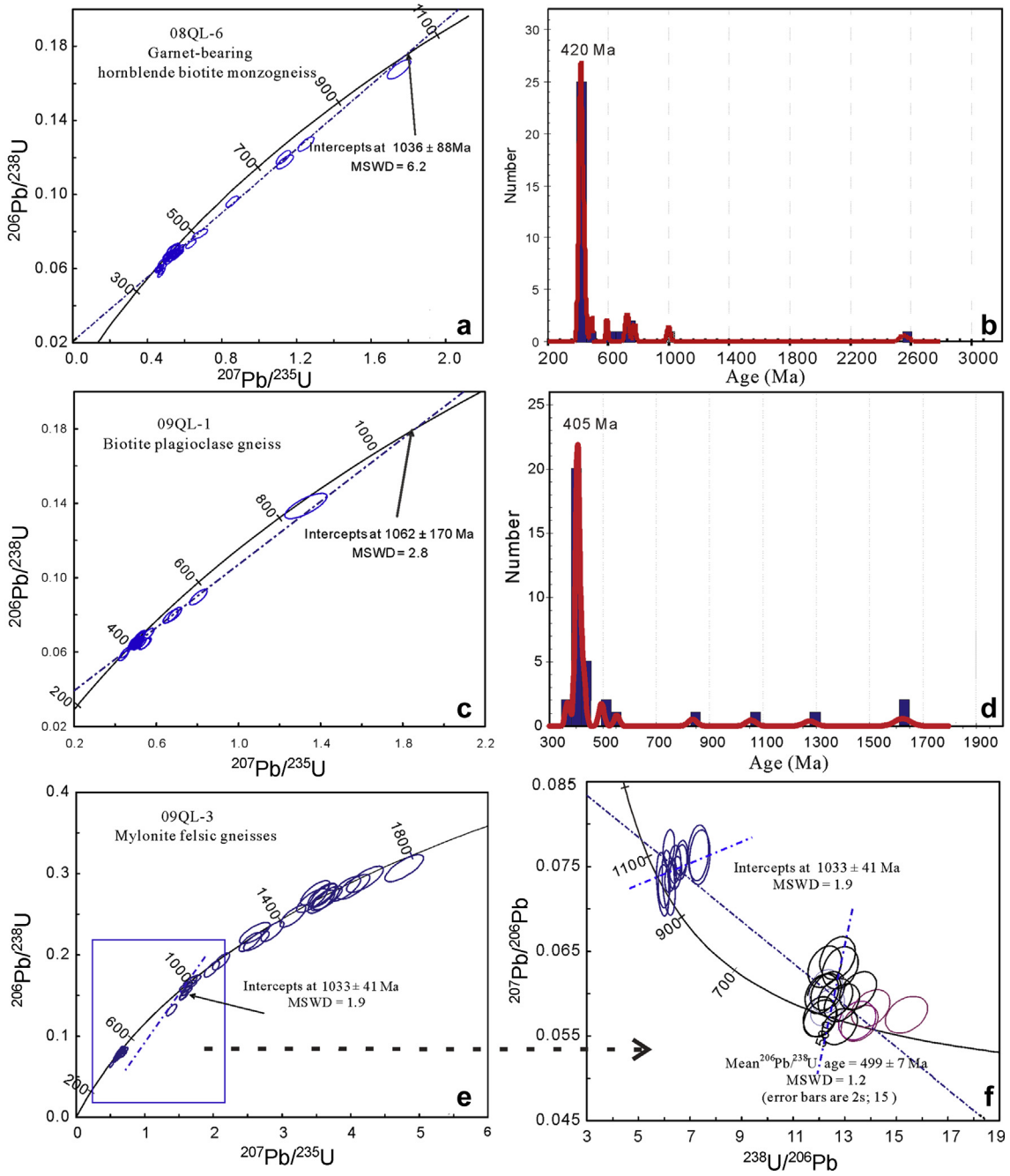

Figure 5. Zircon U-Pb dates for metasedimentary rocks from the Qinling Complex.

and molecular MgO/(MgO + FeO^t) × 100 of 31.0–48.6. The rocks are low in Ni (4–13 ppm) and Cr (9–37 ppm), and enriched in LREEs, with $(La/Yb)_N$ ratios of 4.7–9.9; they show negative Eu anomalies (Eu/Eu* values of 0.56–0.81) (Fig. 10c). On a PM-normalized trace element diagram, they display enrichment in large ion lithophile elements, such as Rb, Ba, Th, U, and Sr, and depletion in high field strength elements (negative Nb, Ta, P, and Ti anomalies) (Fig. 10d).

6. Discussion

6.1. Formation age of the Qinling Complex

The Qinling Complex is regarded as the key unit to understanding the evolution of the NQOB. However, so far, its formation age has remained controversial. Traditionally, the Qinling Complex is considered to have been deposited during the Paleoproterozoic (SBGMR, 1989). Chen et al. (1991) obtained a controversial Sm-Nd whole-rock isochron age of 1.21 Ga for five garnet–amphibole schists collected from the lower unit of the Qinling Complex, suggesting that the protoliths of the Qinling Complex are of Mesoproterozoic age. Zhang et al. (1994) obtained an upper intercept zircon U-Pb age of 2226 Ma from a biotite plagioclase gneiss (of metasedimentary origin) from the Shewei area, Xixia County, by means of an isotope dilution thermal ionization mass spectrometry method; they interpreted that the Qinling Complex formed in the Paleoproterozoic (Zhang et al., 1994). Using SHRIMP and LA-ICP-MS zircon U-Pb methods, Lu et al. (2006) dated detrital zircons from a sillimanite-bearing biotite quartz schist collected from the Zhaigen

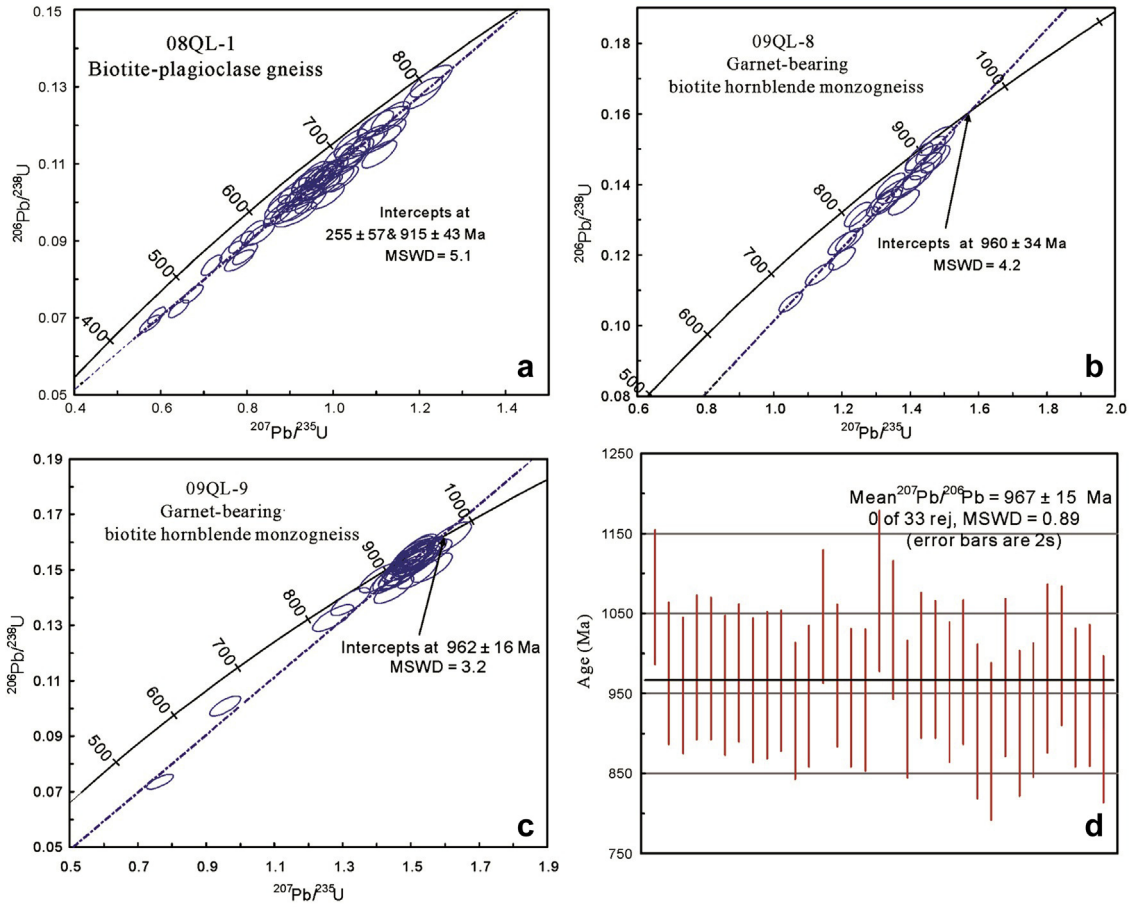

Figure 6. Zircon U-Pb dates for Neoproterozoic granitic gneisses.

area; they believed that the metasedimentary rocks of the Qingling Complex must have been deposited during 1500–960 Ma. Recently, Wan et al. (2011a) re-dated samples that were previously analyzed by Zhang et al. (1994); 56 analyses of 47 zircons gave ages ranging from >3.0 to ca. 400 Ma; they argued that the protoliths of the metasedimentary rocks of the Qinling Complex were formed after the Paleoproterozoic, with some probably being late Mesoproterozoic or even later in age.

In this study, three metasedimentary samples (08QL-6, 09QL-1, and 09QL-3) contained zircons with complex core–rim structures, inherited cores showing oscillatory or planar zoning, and zircons occurring as stubby to elongated shapes with inherited cores that lack zoning (Fig. 4a–c), suggesting that they are magmatic zircons that experienced different degrees of solid-state recrystallization (Hoskin and Black, 2002; Wu et al., 2007). Metamict areas in zircon crystals are susceptible to trace element loss, including loss of radiogenic Pb, which is responsible for their observed discordant ages (Hoskin and Black, 2002; Wu et al., 2007). They yield upper intercept ages of 1036, 1062, and 1033 Ma (Fig. 5a, c, e), which are interpreted as minimum ages of the detrital zircons, and reveal that sedimentary rocks of the Qinling Complex were deposited at some time after ca. 1062 Ma. On the other hand, LA-ICP-MS U-Pb analyses reveal that the granitoid gneisses in the Qinling Complex were emplaced at 962–915 Ma (Fig. 6), thus constraining the depositional age of the Qinling Complex to earlier than 962–915 Ma. Taken together, the formation age of the Qinling Complex can be constrained to the period between the late Mesoproterozoic and early Neoproterozoic (ca. 1062–962 Ma), rather than the Neoproterozoic as previously considered.

6.2. Metamorphic ages of the Qinling Complex

The available data show that the high- and ultra-high pressure (HP-UHP) rocks in the NQOB occur as lenses or boudins in gneisses of the Qinling Complex (Wang et al., 2011, 2013a,b; Liu et al., 2013c; Wang and Wu, 2013). The P–T conditions of eclogite-facies metamorphism are restricted to 2.25–3.0 GPa and 630–770 °C based on conventional thermobarometry and pseudo-section estimates (Zhang et al., 2011; Cheng et al., 2012). Their peak metamorphic ages were refined to ca. 510–490 Ma (Liu et al., 2013c; Wang and Wu, 2013). In this study, the metamorphic zircons of mylonitized felsic gneiss obtained from the Shewei area record abundant metamorphic ages of 499 ± 7 Ma (Fig. 5e, f), which is consistent with the peak metamorphic age of HP-UHP rocks (within analytical errors). Recently, a felsic orthogneiss and an amphibolite from the Qinling Complex, collected in the same area, were dated using SIMS zircon U-Pb methods, yielding lower intercept ages of 505 ± 70 and 498 ± 20 Ma, respectively, which are interpreted as the metamorphic ages of the two samples (Liu et al., 2013a). This evidence indicates that both the HP-UHP rocks and their country rocks (the Qinling Complex) experienced intensive regional metamorphism during the Ordovician.

In the field, the Qinling Complex occurs as banded gneisses, augen gneisses, and vein-structured gneisses, which indicate that they are migmatites that were partially melted during orogenesis of the NQOB. Generally speaking, the core region of the NQOB (i.e., the Xixia area) experienced more intensive metamorphism and migmatization, the intensity decreasing from north to south and from west to east. During crustal partial melting, metamorphic zircons

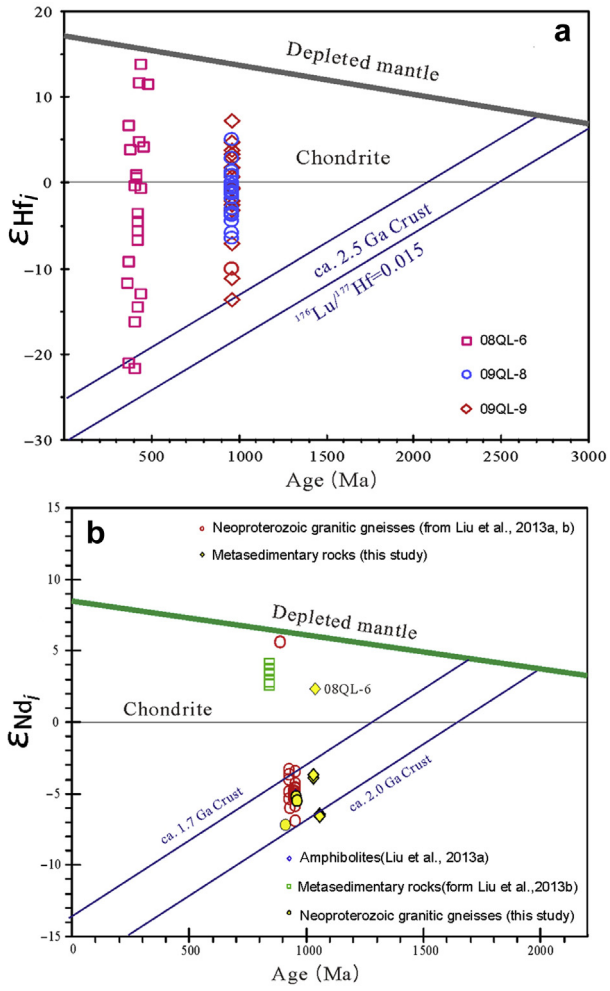

Figure 7. Plots of $\varepsilon_{Hf}(t)$) versus age (a) and $\varepsilon_{Nd}(t)$ versus age (b) for Qinling complex and Neoproterozoic granitic gneisses.

are formed by a range of processes, including: (1) dissolution and re-precipitation of pre-existing zircons; (2) Zr and Si release by metamorphic breakdown reactions of Zr-bearing major silicates and accessory phases other than zircons in a closed system; and (3) crystallization from externally derived Zr-bearing melts (Hoskin and Black, 2002; Brown, 2007; Wu et al., 2007). Therefore, the U-Pb isotopic system of preexisting zircons was completely or partly disturbed during anatectic melting, and new metamorphic zircons corresponding to subsequent significant metamorphic processes occur as overgrowths around inherited pristine cores (Hoskin and Black, 2002; Scherstén et al., 2004; Brown, 2007; Wu et al., 2007).

It has been documented that U-Pb dating of in situ zircons is a more powerful technique than traditional Ar-Ar, Rb-Sr, and Sm-Nd chronometers for obtaining reliable ages of high-grade metamorphic rocks (Jahn et al., 2005). In the metasedimentary samples 08QL-6 and 09QL-1, CL images of zircons reveal that they can be divided into two groups (Fig. 4a, b), a group with pristine cores and a group exhibiting obvious core–rim structures. The zircons with inherited pristine cores have undergone variable degrees of radioactive Pb loss, suggesting that they suffered different degrees of recrystallization; the majority of these zircons have white or black metamorphic rims. The zircons without cores show weak or no zoning, and are interpreted as typical of metamorphic zircons formed during partial crustal melting (Hoskin and Black, 2002; Brown, 2007; Wu et al., 2007). The LA-ICP-MS U-Pb data show that the metamorphic zircons and the newly formed metamorphic rims record two major age peaks, of ca. 420 and ca. 400 Ma (Fig. 5b, d). Therefore, the metamorphism and migmatization of the Qinling Complex occurred at ca. 420–400 Ma (late Silurian to early Devonian).

6.3. Characteristics of Neoproterozoic granitoids

In the NQOB, nearly all Neoproterozoic granitoids have been recognized in the Qinling Complex, and these Neoproterozoic granitoids can be grouped into two stages, ca. 979–914 and ca. 844 Ma. Granitoids of the first stage consist of 13 plutons, which from west to east are exposed in the Lijiazhuang, Yuanlong (Pei et al., 2007), Xinyang (Pei et al., 2007), and Guojiaping (Lu et al., 2005) areas of Gansu Province; the Lianghekou (Chen et al., 2006), Xilaoyu (Chen et al., 2006), and Caiao (Zhang et al., 2004) areas of Shanxi Province; and the Niujiaoshan (Wang et al., 2005), Zhaigen (Chen et al., 2006), Shicaogou (Cheng et al., 2004), Dehe (Cheng et al., 2004; Liu et al., 2013b), and Fangzhuang (Liu et al., 2013a) areas of Henan Province. In addition, we reported two Neoproterozoic granitoid plutons with LA-ICP-MS zircon ages of 915 and ca. 960 Ma, from the Fengyu area of Shanxi Province and the Shewei area of Henan Province, respectively.

Generally, the first-stage Neoproterozoic granitoids in the NQOB present the following characteristics: (1) they consist of biotite granite, biotite–muscovite monzogranites, and monzogranites, containing mainly plagioclase, K-feldspar, quartz, biotite, and muscovite with minor amounts of garnet, apatite, Fe-Ti oxides, and zircon. (2) Most of the plutons are strongly deformed, displaying gneissic structures or mylonitic fabrics with gneissic structures; they are characterized by a nearly WNW–SSE trending penetrative foliation and mineral lineation with long axes parallel to the regional foliation, suggesting that they probably underwent the same deformational event that resulted in the development of the regional foliation in the NQOB (Wang et al., 2002, 2003, 2005; Lu et al., 2005). (3) Geochemically, these rocks are typically high-K calc-alkaline rocks with A/CNK values of 1.00–1.13. Large variations in their chemical compositions suggest a transition in magmatic evolution from S-type-like to I-type-like magmas (Fig. 10b). (4) Most of the rocks show negative whole-rock $\varepsilon_{Nd}(t)$ values and negative Hf-in-zircon $\varepsilon_{Hf}(t)$ values (−9.3 to −10.6) (Fig. 7a, b) with elevated $\delta^{18}O$ values (10.9–11.7) (Liu et al., 2013a). Their corresponding Hf model ages are significantly older than their crystallization ages, indicating that these rocks formed from the partial melting of ancient continental crust (Fig. 7a, b). (5) These granitoids were emplaced in a syn- or post-collisional orogenic setting (Liu et al., 2013b; Wang et al., 2013a,b), which is interpreted to represent the formation of the Rodinia supercontinent.

The second-stage Neoproterozoic granitoids are recognized in the NQOB only in the Fangcheng area. They are dominated by A-type granitoids and consist mainly of nepheline syenite, aegirine syenite, and alkali-feldspar syenite. An age of 844 ± 2 Ma was determined by LA-ICP-MS zircon U-Pb dating, geochemical characters indicated that the Fangcheng alkali syenites are derived from the melting of a small proportion of upper mantle in an extensional regime in an intraplate orogenic setting (Bao et al., 2008).

6.4. Tectonic setting of the Qinling Complex

The tectonic setting of the Qinling Complex has been controversial. Most researchers believe that the complex formed in a continental rift environment (Xiao et al., 1988; Gao et al., 1996; Zhang et al., 2002), an interpretation that is based mainly on the chemical compositions of metagreywackes. Some researchers have

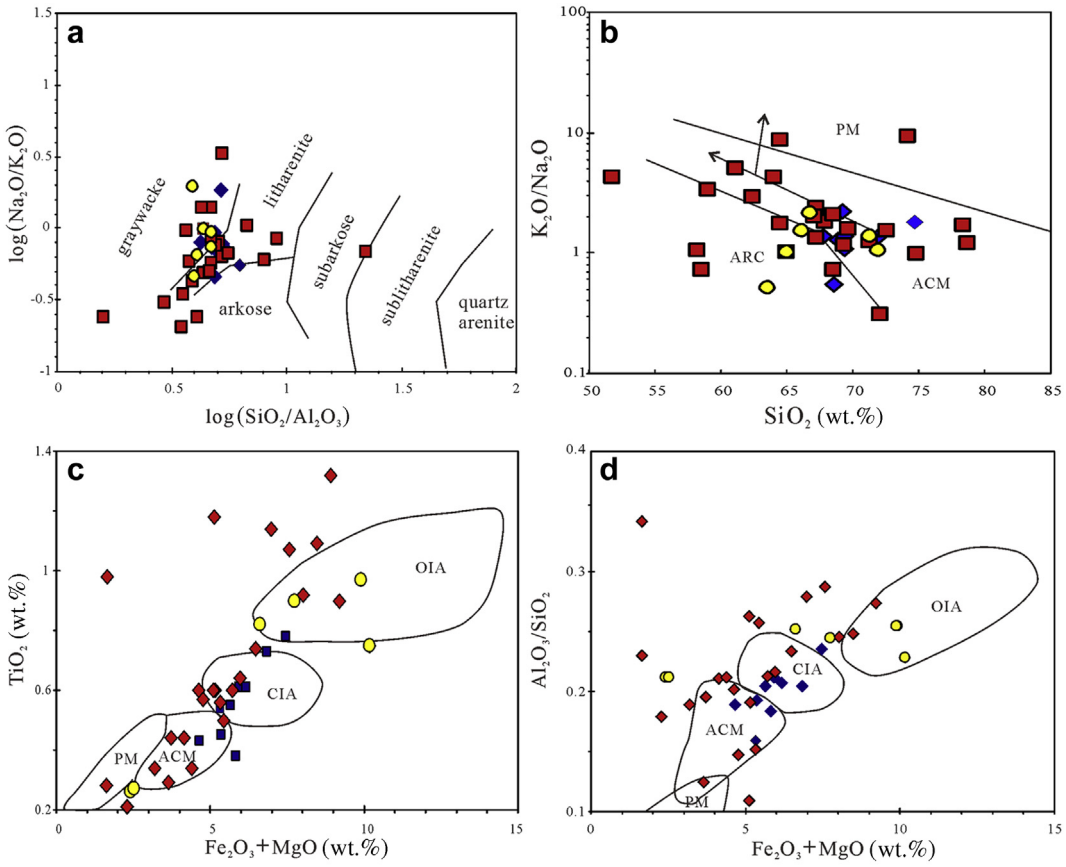

Figure 8. (a) Geochemical classification of metasedimentary rocks from the Qinling Complex (after Pettijohn et al., 1987). (b)–(d) Tectonic discrimination diagrams for metasedimentary rocks from the Qinling Complex. (b) is after Roser and Korsch (1988); (d) is after Bhatia and Crook (1986). PM = passive margin; ACM = active continental margin; ARC = oceanic island arc; CIA = continental island arc; OIA = oceanic island arc. Data are from You et al. (1991) (blue square), Chen (2007) (red diamond) and this study (yellow circle).

proposed that the metasediments of the Qingling Complex were deposited on a Proterozoic active continental margin (You et al., 1991). In addition, some researchers have suggested, based on an integrated geochemical approach, that felsic paragneisses of the Qinling Complex were probably deposited in a Neoproterozoic volcanic arc environment (Liu et al., 2013a).

Lithologically, the Qinling Complex consists of metagraywackes and marbles with some amphibolites. Two types of amphibolite can be recognized (You et al., 1991; Yan et al., 2009): those which show intrusive contacts with host rocks, and which were mainly derived from metabasic intrusives, and those which occur intercalated with marble, probably derived from marly limestones (You et al., 1991; Yan et al., 2009). Some amphibolites are far younger than previously thought, as SHRIMP U-Pb ages of zircons show that they formed during the late Ordovician (449 ± 11 Ma) (Yan et al., 2009). Hence, it ought to be impossible to discriminate the tectonic settings of the Qinling Complex by using data from the amphibolites. Furthermore, Zhang et al. (2001) considered that the gneisses and

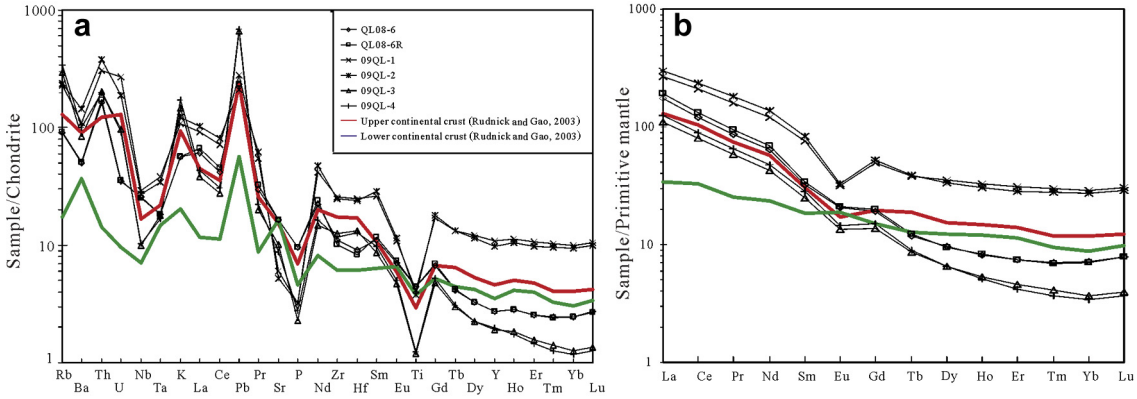

Figure 9. Chondrite-normalized REE patterns and primitive-mantle-normalized trace element diagrams of metasedimentary rocks from the Qinling Complex. Chondrite and PM values are from Sun and McDonald (1989); upper and lower continental crust values are from Rudnick and Gao (2003).

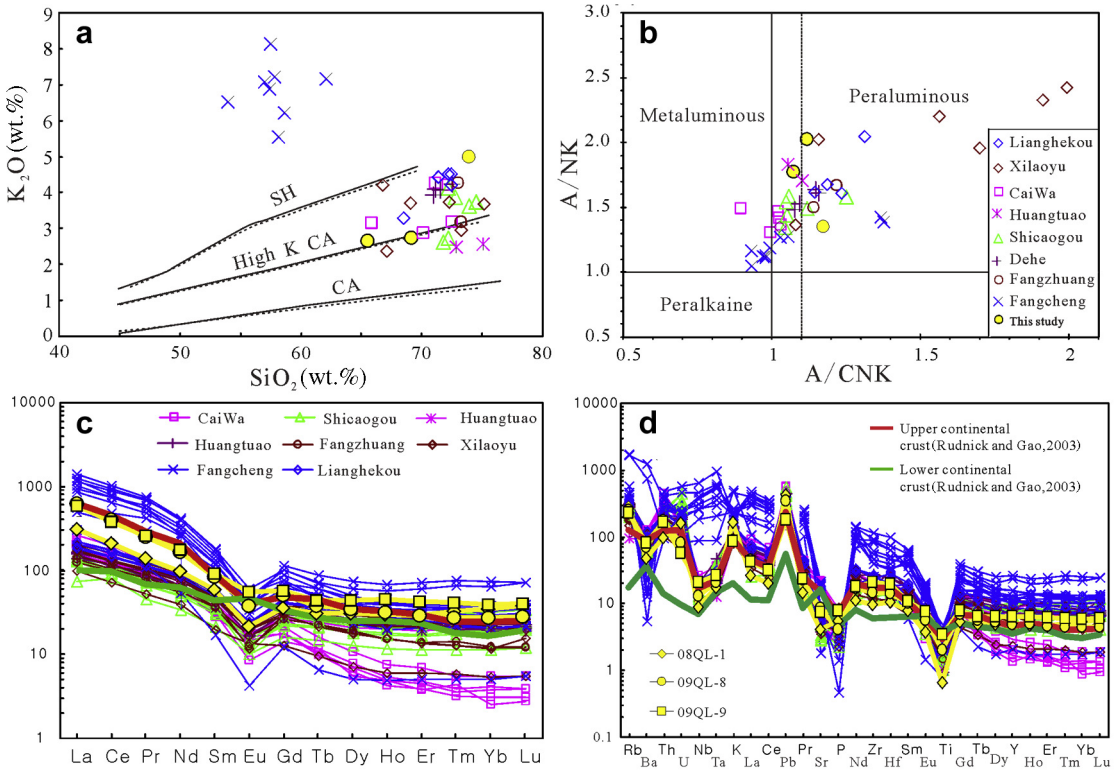

Figure 10. (a) SiO_2 versus K_2O diagram. (b) Plot of A/CNK versus A/NK (A/NK = molar ratio of $Al_2O_3/(Na_2O + K_2O)$; A/CNK = molar ratio of $Al_2O_3/(CaO + Na_2O + K_2O)$). (c) Chondrite-normalized REE patterns. (d) Primitive-mantle-normalized trace element diagrams for the Neoproterozoic granitic gneisses. Chondrite and PM values are from Sun and McDonald (1989). Data are from Yang et al. (1992), Lu et al. (2003), Chen et al. (2006), Zhang et al. (2004), Chen et al. (2007), Bao et al. (2008), Liu et al. (2013b) and this study.

marbles of the Qinling Complex were assembled tectonically rather than by a continuous sedimentary process (You et al., 1991); if this is true, the marbles should be excluded from the complex.

The metasedimentary rocks of the Qinling Complex contain high feldspar contents (generally, ~40%) and their protoliths are dominated by graywackes and litharenites (Fig. 8a). Given that feldspars and lithic arenite fragments are chemically and physically unstable and thus less likely to survive recycling than other minerals such as quartz, it is inferred that the sediments of the Qinling Complex were poorly sorted and immature, and were supplied from a rapidly uplifted region. Girty et al. (1996) proposed that Al_2O_3/TiO_2 values of sediments can serve as an index to discriminate sediments derived from different provenances. Rocks with Al_2O_3/TiO_2 ratios of 18–24 are likely derived from old differentiated upper continental crust; Al_2O_3/TiO_2 values for basalt vary between ~5 and 14, whereas sediments with variable Al_2O_3/TiO_2 values (17–50) could be derived from andesites to rhyolites and/or their plutonic equivalents in magmatic arc settings. The available data show that the metasedimentary rocks of the Qinling Complex present a large range of Al_2O_3/TiO_2 values, of 14.3–62.1, indicating a mixed provenance and depositional setting on a typical active continental margin, in contrast to a passive continental margin where sediments are commonly derived from weathering of a magmatic arc (Girty et al., 1996). On K_2O/Na_2O–SiO_2 plots (Roser and Korsch, 1988), most Qinling Complex samples fall within the active continental margin and oceanic island arc fields (Fig. 8b). On TiO_2 (in wt.%) versus Fe_2O_3 + MgO (in wt.%) and Al_2O_3/SiO_2 versus Fe_2O_3 + MgO (in wt.%) plots (Fig. 8c, d) (Bhatia and Crook, 1986), the samples from the Qinling Complex are scattered across a wide range of environments, including the active continental margin, continental island arc, and oceanic island arc fields, suggesting a wide range of source rocks, which is also consistent with an active margin setting. In addition, some relatively immobile trace elements of sedimentary rocks, such as La, Y, Th, Zr, Hf, Nb, Ti, and Sc, have proven useful in determining tectonic settings (Bhatia and Crook, 1986). On La–Th–Sc and Th–Sc–Zr/10 ternary plots (Fig. 11), the metasedimentary rocks of the Qinling Complex mainly fall within the active continental margin field. The Qinling Complex shows pronounced negative Nb–Ta anomalies (Fig. 9), clearly indicative of a subduction-related magmatic source. Taken together, the Qinling Complex is mostly affiliated with subduction–accretion along an active continental margin, with detrital components having been deposited along an active continental margin (Dickinson, 1995).

6.5. Precambrian history of the NQOB

It is generally accepted that the Qinling Orogenic Belt is divided into north and south belts by the Shangdan suture zone. However, the tectonic affinities of the NQOB remain debated. Some researchers have proposed that the NQOB has tectonic affinities with the NCC, and that it behaved as an active continental margin along the southern margin of the NCC in the early Paleozoic (Zhang et al., 1996b, 2001; Dong et al., 2011b). Based on geochemical characteristics, some researchers considered that the NQOB, which is distinct from the NCC, is similar to the Yangtze craton and the South Qinling belt (Zhang et al., 1996a, 2002). Others have argued that the NQOB was an independent micro-continent during the Precambrian (Xu et al., 1997; Dong et al., 2008; Diwu et al., 2010, 2012).

The NCC consists of uniform Archean to Paleoproterozoic metamorphosed basement, overlain by Mesoproterozoic to Phanerozoic unmetamorphosed sedimentary cover (Zhai et al., 2005; Zhai and Santosh, 2011; Zhao and Zhai, 2013). The basement rocks present age peaks at ~2.52 and ~1.85 Ga (Wan et al., 2011b;

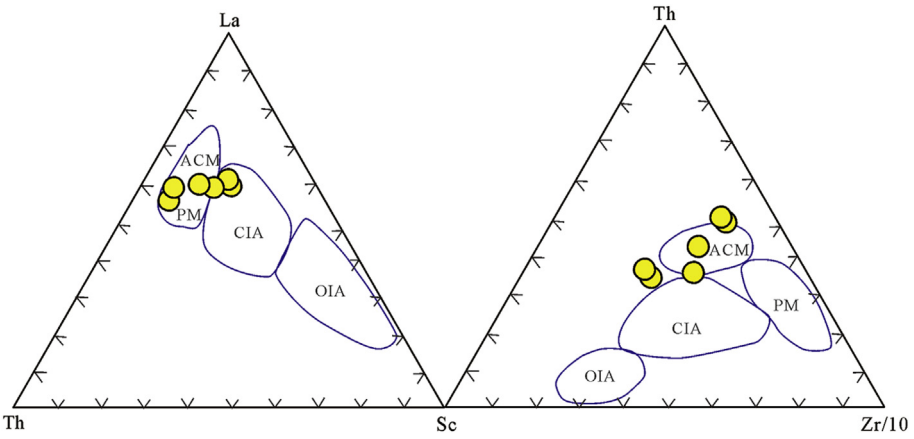

Figure 11. Triangular trace element plots for metasedimentary rocks from the Qinling Complex (after Bhatia and Crook, 1986). Abbreviations as in Fig. 8.

Diwu et al., 2012b). The U-Pb ages of detrital zircons from modern rivers on the NCC do not show an ca. 1.0 Ga age peak (Yang et al., 2009; Diwu et al., 2012a). In contrast, in South China especially, the Yangtze Craton is characterized by middle Neoproterozoic basement rocks with sporadic occurrences of Paleoproterozoic to Archean rocks, showing a predominant Neoproterozoic magmatic event at ca. 830 Ma (Liu et al., 2008).

Detrital zircon grains from metasedimentary rocks and modern river sands in the NQOB yielded detrital zircon age populations of 1.0–0.85 Ga with a peak at 980 Ma (Diwu et al., 2010, 2012; Zhu et al., 2011), which is closely tied to the formation of the Rodinia supercontinent (Li et al., 2008; Santosh et al., 2009). Abundant early Neoproterozoic rocks are also recognized in this region. The Songshugou ophiolite, which was emplaced in the south of the Qinling Complex, and mafic rocks of the ophiolite mainly show E-MORB and T-MORB trace element patterns, with a Sm-Nd isochron age of 1030 ± 46 Ma (Dong et al., 2008). The metamafic rocks of the Kuanping Complex are characterized by N-MORB trace element patterns, with a zircon U-Pb age of 943 ± 6 Ma (Diwu et al., 2010) and a whole-rock Sm-Nd isochron age of 1142 ± 18 Ma (Zhang and Zhang, 1995). Some researchers have proposed that the metamafic rocks of the complex represent a dismembered ophiolite, with an age ranging from 1.14 to 0.94 Ga (Diwu et al., 2010). Furthermore, an increasing number of Neoproterozoic granitic plutons have been reported from the NQOB, which were intruded into the Qinling Complex between 980 and 930 Ma; these granites can be interpreted as the products of syn- and post-collisional processes, which could be a response to the assembly of Rodinia in the early Neoproterozoic (Lu et al., 2003; Wang et al., 2003; Chen et al., 2006; Liu et al., 2013a, b; Wang et al., 2013a,b). Therefore, all of the above observations suggest that the NQOB was an independent micro-continent, at least prior to the Neoproterozoic, and that it was a portion of the Grenville orogenic belt during 1.2–0.8 Ga, with a peak age at ca. 1.0 Ga. These features reveal its unique geological history, which is clearly different from that of the NCC and the Yangtze Craton during the Precambrian (Diwu et al., 2010, 2012).

Li et al. (2008) proposed that the Rodinia supercontinent was assembled during worldwide orogenic events between 1300 Ma and 900 Ma. Rodinia lasted for about 150 Myr after complete assembly. The breakup of Rodinia occurred between ca. 825 Ma and 740 Ma. Recently, Liu et al. (2013a,b,c) reported a U-Pb zircon SIMS age of an amphibolite dyke intruded into the Qinling Complex in the Xixia area, with an upper intercept age of 845 ± 69 Ma and a lower intercept age of 517 ± 71 Ma, suggesting that the dyke intruded during the Neoproterozoic and suffered metamorphism during a later Paleozoic thermotectonic event. The HP and UHP rocks of the NQOB occur as lenses, blocks, and layers in the Qinling Complex. A large amount of zircon U-Pb data reveals that these HP and UHP rocks have protolith ages of ca. 830–740 Ma (Wang et al., 2011, 2013a,b; Wang and Wu, 2013). Geochemical data show that the protoliths of the HP and UHP rocks are characterized by tholeiitic bulk compositions, EMORB-like trace element patterns, and high positive whole-rock $\varepsilon_{Nd}(t)$ and zircon $\varepsilon_{Hf}(t)$ values, all of which in turn indicate that they formed in a continental rift setting (Wang et al., 2013a,b; Wang and Wu, 2013). Even detrital zircons in modern rivers record a predominant ca. 825 Ma age peak for the NQOB. All of these observations suggest that the NQOB separated from the Rodinia supercontinent at ca. 830–740 Ma.

Subsequently, the NQOB moved closer to the northern margin of the NCC, and their initial accretion or collision occurred during the late Cambrian to the early Ordovician (Diwu et al., 2012). Wu and Zheng (2013) suggested that this event was caused by northward subduction of the North Qinling microcontinent beneath the Erlangping arc. It has been assumed that the North Qinling rocks were subducted to mantle depths of at least 80–120 km to undergo UHP metamorphism. However, Dong et al. (2011b) believed that the Erlangping back-arc basin was subducted towards the south under the North Qingling terrane during this period, which is indicated by the formation of UHP-HP metamorphic rocks. Meanwhile, 507–470 Ma granitoid rocks intruded into the Qinling Complex and adjacent areas (Wang et al., 2013a,b; Zhang et al., 2013), an event that was contemporaneous with the ca. 500 Ma HP-UHP metamorphism. Those granitoids are the products of S-type magma, suggesting that they formed mainly by partial melting of clastic rocks of the NQOB (Zhang et al., 2013).

Orogenic belts generally experience a transition in tectonic regime from overall crustal thickening to extensional thinning. The onset of extensional tectonics causes an increase in heat-flow-associated crustal thinning, which is marked by partial melting of orogenic crust, resulting in migmatites, regional metamorphism, and granite intrusions (Foster et al., 2001; Keay et al., 2001; Wu et al., 2007). In the NQOB, the Qinling Complex suffered intensive and widespread migmatization, and in our study, the metamorphic zircons of the Qinling Complex give U-Pb ages of ca. 420–400 Ma, which can constrain the time of partial melting in this region. As previous studies show that three major magmatic events occurred in the NQOB during the early Paleozoic (Wang et al., 2013a,b; Bader et al., 2013; Zhang et al., 2013), zircon U-Pb dating of those granitoids yields three age peaks of ca. 500, 452 and 420 Ma, correlating with HP to UHP metamorphism at ca. 500 Ma, retrograde granulite-facies metamorphism at ca. 450 Ma, and amphibolite-facies

metamorphism at ca. 420 Ma, respectively (Zhang et al., 2013). Therefore, the magmatism, migmatization, and metamorphism in the NQOB are related to the transition of the tectonic regime from compression to extension during the late Silurian to early Devonian. The metamorphism and migmatization may have been caused by the emplacement of voluminous granitoid rocks.

7. Conclusions

The formation age of the Qinling Complex can be constrained to the period between the late Mesoproterozoic and early Neoproterozoic (ca. 1062–962 Ma), rather than to the Paleoproterozoic as previously thought. The complex was mostly deposited along an active continental margin in a forearc basin setting.

The LA-ICP-MS zircon U-Pb data show that the Qinling Complex recorded two major metamorphic ages, of ca. 499 Ma and ca. 420–400 Ma. The former is consistent with the peak metamorphic ages of HP-UHP rocks in the Qinling Complex; the latter can constrain the time of partial melting in the NQOB during the late Silurian to early Devonian.

The available data indicate that the NQOB was an independent micro-continent prior to the Neoproterozoic, and that it was once a portion of the Grenville orogenic belt, during ca. 1.2–0.8 Ga. The NQOB separated from the Rodinia supercontinent at ca. 830–740 Ma. Subsequently, the NQOB moved closer to the northern margin of the NCC, and their initial accretion or collision occurred during the late Cambrian to early Ordovician.

Acknowledgments

This paper honors the distinguished geologists Guowei Zhang and Alfred Kröner for their outstanding contributions to continental evolution. This research was financially supported by the Natural Science Foundation of China (Grant Nos. 41090374 and 41272004) and MOST Special Funds from the State Key Laboratory of Continental Dynamics. Diwu thanks Prof M. Santosh for the opportunity to contribute to this special issue and his speedy handling of the paper. We thank the two anonymous journal reviewers for their critical comments which greatly benefited to the manuscript.

Appendix A. Supplementary data

Supplementary data related to this article can be found at http://dx.doi.org/10.1016/j.gsf.2014.04.001

References

Albarède, F., Scherer, E.E., Blichert-Toft, J., Rosing, M., Simionovici, A., Bizzarro, M., 2006. γ-ray irradiation in the early solar system and the conundrum of the 176Lu decay constant. Geochimica et Cosmochimica Acta 70, 1261–1270.

Bader, T., Franz, L., Ratschbacher, L., de Capitani, C., Webb, A.A.G., Yang, Z., Pfänder, J.A., Hofmann, M., Linnemann, U., 2013. The heart of China revisited: II early Paleozoic (ultra) high-pressure and (ultra)high-temperature metamorphic Qinling orogenic collage. Tectonics 32, 922–947.

Bao, Z., Wang, Q., Bai, G., Zhao, Z., Song, Y., Liu, X., 2008. Geochronology and geochemistry of the Fangcheng Neoproterozoic alkali-syenites in East Qinling orogen and its geodynamic implications. Chinese Science Bulletin 53, 2050–2061.

Bhatia, M., Crook, K.W., 1986. Trace element characteristics of graywackes and tectonic setting discrimination of sedimentary basins. Contributions to Mineralogy and Petrology 92, 181–193.

BlichertToft, J., Albarede, F., 1997. The Lu-Hf isotope geochemistry of chondrites and the evolution of the mantle-crust system. Earth and Planetary Science Letters 148, 243–258.

Brown, M., 2007. Crustal melting and melt extraction, ascent and emplacement in orogens: mechanisms and consequences. Journal of the Geological Society 164, 709–730.

Chen, Q., 2007. Chemical ages for the multi-stage metamorphism of the Qinling Group at Taibai, Shaanxi province. Master Thesis. China University of Geosciences, Wuhan, pp. 1–49.

Chen, N., Han, Y., You, Z., Sun, M., 1991. Whole rock Sm–Nd, Rb–Sr and single zircon Pb–Pb dating of complex rocks from the interior of the Qinling orogenic belt, western Henan and its crustal evolution. Geochemica 3, 219–228.

Chen, Z., Lu, S., Li, H., Li, H., Xiang, Z., Zhou, H., Song, B., 2006. Constraining the role of the Qinling orogen in the assembly and break-up of Rodinia: tectonic implications for Neoproterozoic granite occurrences. Journal of Asian Earth Sciences 28, 99–115.

Cheng, H., Zhang, C., Vervoort, J.D., Li, X., Li, Q., Wu, Y., Zheng, S., 2012. Timing of eclogite facies metamorphism in the North Qinling by U–Pb and Lu–Hf geochronology. Lithos 136–139, 46–59.

Cheng, Z., Lu, S., Li, H., Song, B., Li, H., Xiang, Z., 2004. The age of the Dehe biotite monzogranite gneiss in the North Qinling: TIMS and SHRIMP U-Pb zircon dating. Geological Bulletin of China 23, 136–141.

Chu, N.-C., Taylor, R.N., Chavagnac, V.r., Nesbitt, R.W., Boella, R.M., Milton, J.A., German, C.R., Bayon, G., Burton, K., 2002. Hf isotope ratio analysis using multi-collector inductively coupled plasma mass spectrometry: an evaluation of isobaric interference corrections. Journal of Analytical Atomic Spectrometry 17, 1567–1574.

Dickinson, W.R., 1995. Forearc basins. In: Busby, C.J., Ingersoll, R.V. (Eds.), Tectonics of Sedimentary Basins. Blackwell Science, Cambridge, pp. 221–261.

Diwu, C., Sun, Y., Liu, L., Zhang, C., Wang, H., 2010. The disintegration of Kuanping Group in North Qinling orogenic belts and neo-proterozoic N-MORB. Acta Petrologica Sinica 26, 2025–2038.

Diwu, C., Sun, Y., Zhang, H., Wang, Q., Guo, A., Fan, L., 2012. Episodic tectonothermal events of the western North China Craton and North Qinling Orogenic Belt in central China: constraints from detrital zircon U-Pb ages. Journal of Asian Earth Sciences 47, 107–122.

Dong, Y.P., Zhou, M.F., Zhang, G.W., Zhou, D.W., Liu, L., Zhang, Q., 2008. The Grenvillian Songshugou ophiolite in the Qinling Mountains, Central China: Implications for the tectonic evolution of the Qinling orogenic belt. Journal of Asian Earth Sciences 32, 325–335.

Dong, Y., Zhang, G., Hauzenberger, C., Neubauer, F., Yang, Z., Liu, X., 2011a. Palaeozoic tectonics and evolutionary history of the Qinling orogen: evidence from geochemistry and geochronology of ophiolite and related volcanic rocks. Lithos 122, 39–56.

Dong, Y., Zhang, G., Neubauer, F., Liu, X., Genser, J., Hauzenberger, C., 2011b. Tectonic evolution of the Qinling orogen, China: review and synthesis. Journal of Asian Earth Sciences 41, 213–237.

Foster, D.A., Schafer, C., Fanning, C.M., Hyndman, D.W., 2001. Relationships between crustal partial melting, plutonism, orogeny, and exhumation: Idaho–Bitterroot batholith. Tectonophysics 342, 313–350.

Günther, D., Hattendorf, B., 2005. Solid sample analysis using laser ablation inductively coupled plasma mass spectrometry. TrAC Trends in Analytical Chemistry 24, 255–265.

Gao, S., Zhang, B.R., Wang, D.P., Ouyang, J.P., Xie, Q.L., 1996. Geochemical evidence for the Proterozoic tectonic evolution of the Qinling orogenic belt and its adjacent margins of the north China and Yangtze cratons. Precambrian Research 80, 23–48.

Girty, G.H., Ridge, D.L., Knaack, C., Johnson, D., Al-Riyami, R.K., 1996. Provenance and depositional setting of Paleozoic chert and argillite, Sierra Nevada, California. Journal of Sedimentary Research 66, 107–118.

Griffin, W.L., Pearson, N.J., Belousova, E., Jackson, S.E., van Achterbergh, E., O'Reilly, S.Y., Shee, S.R., 2000. The Hf isotope composition of cratonic mantle: LAM-MC-ICP–MS analysis of zircon megacrysts in kimberlites. Geochimica Et Cosmochimica Acta 64, 133–147.

Hoskin, P.W.O., Black, L.P., 2002. Metamorphic zircon formation by solid-state recrystallization of protolith igneous zircon. Journal of Metamorphic Geology 18, 423–439.

Jahn, B.M., Liu, X., Yui, T.-F., Morin, N., Coz, M.B.L., 2005. High-pressure/ultrahigh-pressure eclogites from the Hong'an Block, East-Central China: geochemical characterization, isotope disequilibrium and geochronological controversy. Contributions to Mineralogy and Petrology 149, 499–526.

Keay, S., Lister, G., Buick, I., 2001. The timing of partial melting, Barrovian metamorphism and granite intrusion in the Naxos metamorphic core complex, Cyclades, Aegean Sea, Greece. Tectonophysics 342, 275–312.

Li, Z.X., Bogdanova, S.V., Collins, A.S., Davidson, A., De Waele, B., Ernst, R.E., Fitzsimons, I.C.W., Fuck, R.A., Gladkochub, D.P., Jacobs, J., Karlstrom, K.E., Lu, S., Natapov, L.M., Pease, V., Pisarevsky, S.A., Thrane, K., Vernikovsky, V., 2008. Assembly, configuration, and break-up history of Rodinia: a synthesis. Precambrian Research 160, 179–210.

Liu, B.X., Qi, Y., Wang, W., Siebel, W., Zhu, X.Y., Nie, H., He, J.F., Chen, F., 2013a. Zircon U–Pb ages and O–Nd isotopic composition of basement rocks in the North Qinling Terrain, central China: evidence for provenance and evolution. International Journal of Earth Sciences 102, 2153–2173.

Liu, B., Nie, H., Qi, Y., Yang, L., Zhu, X., Chen, F., 2013b. Genesis and geological significances of Neoproterozoic granitoids in the North Qinling terrain, SW Henan, China. Acta Petrologica Sinica 29, 2437–2455.

Liu, L., Liao, X., Zhang, C., Chen, D., Gong, X., Kang, L., 2013c. Multi-metamorphic timings of HP-UHP rocks in the North Qinling and their geological implications. Acta Petrologica Sinica 29, 1634–1656.

Liu, X., Gao, S., Diwu, C., Ling, W., 2008. Precambrian crustal growth of Yangtze craton as revealed by detrital zircon studies. American Journal of Science 308, 421–468.

Lu, S., Chen, Z., Li, F., Hao, G., Xiang, Z., 2005. Two magmatic belts of the Neoproterozoic in the Qinling Orogenic Belt. Acta Geologica Sinica 79, 165–173.
Lu, S., Chen, Z., Xiang, Z., Li, H., Li, H., Song, B., 2006. Detrital zircon population of Proterozoic metasedimentary strata in the Qinling-Qilian-Kunlun Orogen. Earth Science Frontiers 13, 303–310.
Lu, S., Li, H., Chen, Z., Zhou, H., Guo, J., Niu, G., Xiang, Z., 2003. Meso-Neoproterozoic geological evolution in the Qinling orogeny and its response to the supercontinental events of Rodinia. Geological Publishing House, Beijing, pp. 1–194.
Ludwig, K.R., 2003. Isoplot/Ex Version 2.49. A Geochronological Toolkit for Microsoft Excel. Berkeley Geochronology Center Special Publication No.1a, Berkeley.
Pei, X., Ding, S., Zhang, G., Liu, H., Li, Z., Li, G., Liu, Z., Meng, Y., 2007. The LA-ICPMS zircons U-Pb ages and geochemistry of the Baihua basic igneous complexes in Tianshui area of West Qinling. Science in China Series D-Earth Sciences 50, 264–276.
Pettijohn, F.J., Potter, J.E., Slever, R., 1987. Sand and Sandstone, second ed. Springer-Verlag, pp. 1–5.
Roser, B.P., Korsch, R.J., 1988. Provenance signatures of sandstone-mudstone suites determined using discriminant function analysis of major-element data. Chemical Geology 67, 119–139.
Rudnick, R.L., Gao, S., 2003. 3.01-Composition of the continental crust. In: Heinrich, D.H., Karl, K.T. (Eds.), Treatise on Geochemistry. Pergamon, Oxford, pp. 1–64.
Santosh, M., Maruyama, S., Yamamoto, S., 2009. The making and breaking of supercontinents: some speculations based on superplumes, super downwelling and the role of tectosphere. Gondwana Research 15, 324–341.
SBGMR, 1989. Regional Geology of Shaanxi Province. Geological Publishing House, Beijing, 1–698.
Scherstén, A., Larson, S.Å., Cornell, D.H., Stigh, J., 2004. Ion probe dating of a migmatite in SW Sweden: the fate of zircon in crustal processes. Precambrian Research 130, 251–266.
Shi, Y., Yu, J., Xu, X., Qiu, J., Chen, L., 2009. Geochronology and geochemistry of the Qinling group in the eastern Qinling Orogen. Acta Petrologica Sinica 25, 2651–2670.
Sun, S., McDonald, W.F., 1989. Chemical and isotopic systematics of oceanic basalts: implications for mantle compositions and processes. Magmatism in the Ocean Basins. In: Saunders, A.D., Norry, M.J. (Eds.). Geological Society Special Publications, pp. 42313–42345.
Sun, Y., Lu, X., Han, S., Zhang, G., Yang, S., 1996. Composition and formation of Paleozoic Erlangping ophiolitic slab, North Qinling: evidence from geology and geochemistry. Science in China (D) 39 (Suppl.), 50–59.
Wan, Y., Liu, D., Dong, C., Yin, X., 2011a. SHRIMP zircon dating of meta-sedimentary rock from the Qinling Group in the north of Xixia, North Qinling Orogenic Belt: constraints on complex histories of source region and timing of deposition and metamorphism. Acta Petrologica Sinica 27, 1172–1178.
Wan, Y., Liu, D., Wang, W., Song, T., Kröner, A., Dong, C., Zhou, H., Yin, X., 2011b. Provenance of Meso- to Neoproterozoic cover sediments at the Ming Tombs, Beijing, North China Craton: an integrated study of U–Pb dating and Hf isotopic measurement of detrital zircons and whole-rock geochemistry. Gondwana Research 20, 219–242.
Wang, H., Wu, Y.-B., Gao, S., Liu, X.-C., Liu, Q., Qin, Z.-W., Xie, S.-W., Zhou, L., Yang, S.-H., 2013a. Continental origin of eclogites in the North Qinling terrane and its tectonic implications. Precambrian Research 230, 13–30.
Wang, H., Wu, Y.B., Gao, S., Liu, X.C., Gong, H.J., Li, Q.L., Li, X.H., Yuan, H.L., 2011. Eclogite origin and timings in the North Qinling terrane, and their bearing on the amalgamation of the South and North China Blocks. Journal of Metamorphic Geology 29, 1019–1031.
Wang, H., Wu, Y., 2013. Early Paleozoic HP-UHP metamorphism of the Qinling orogen. Chinese Science Bulletin 58, 1402–1428.
Wang, J., Diwu, C., Sun, Y., Liu, Y., Wang, W., 2012. LA-ICP-MS zricon U-Pb dating and Hf isotope analysis of Qinggangping granodiorite in Xixia area of western Henan province and their geological significance. Geochemical Bulletin of China 31, 884–895.
Wang, T., Wang, X.X., Zhang, G.W., Pei, X.Z., Zhang, C.L., 2003. Rernnants of a Neoproterozoic collisional orogenic belt in the core of the phanerozoic Qinling orogenic belt (China). Gondwana Research 6, 699–710.
Wang, T., Zhang, G., Pei, X., Zhang, C., Li, W., 2002. Possibility of the existence of a Neoproterozoic NW trending orogenic belt in the North Qinling and convergence and breakup of blocks on its two sides. Geological Bulletin of China 21, 516–522.
Wang, T., Zhang, Z., Wang, X., Wang, P., Zhang, C., 2005. Neoproterozoic collisional deformation in the core of the Qinling Orogen and its age: constrained by Zircon SHRIMP dating of strongly deformed syn-collisional granites and weakly deformed granitic veins. Acta Geologica Sinica 79, 220–231.
Wang, X., Hua, H., Sun, Y., 1995. A study on microfossils of the Erlangping Group in Wantan area, Xixia county, Henan province. Geological Magazine, 837–848.
Wang, X., Wang, T., Zhang, C., 2013b. Neoproterozoic, Paleozoic, and Mesozoic granitoid magmatism in the Qinling Orogen, China: constraints on orogenic process. Journal of Asian Earth Sciences 72, 129–151.
Wiedenbeck, M., Hanchar, J.M., Peck, W.H., 2004. Further characterisation of the 91500 zircon crystal. Geostandards and Geoanalytical Research 28, 9–39.
Wu, F.Y., Yang, Y.H., Xie, L.W., Yang, J.H., Xu, P., 2006. Hf isotopic compositions of the standard zircons and baddeleyites used in U-Pb geochronology. Chemical Geology 234, 105–126.
Wu, Y.B., Zheng, Y.F., 2013. Tectonic evolution of a composite collision orogen: an overview on the Qinling-Tongbai-Hong'an-Dabie-Sulu orogenic belt in central China. Gondwana Research 23, 1402–1428.
Wu, Y.B., Zheng, Y.F., Zhang, S.B., Zhao, Z.F., Wu, F.Y., Liu, X.M., 2007. Zircon U-Pb ages and Hf isotope compositions of migmatite from the North Dabie terrane in China: constraints on partial melting. Journal of Metamorphic Geology 25, 991–1009.
Xiao, S., Zhang, W., Song, Z., 1988. The Metamorphic Strata of the Northern Qinling in China. Xi'an Jiaotong University Press, Xi'an, 1–320.
Xu, J., Zhang, B., Han, Y., 1997. Discovery of high radiogenic Pb isotopic composition from Proterozoic mafic rocks in North Qinling area and its implication. Chinese Science Bulletin 42, 51–54.
Yan, Q., Wang, Z., Yan, Z., Chen, J., Xiang, Z., Wang, T., Zhang, H., 2009. Tectonic affinity and timing of two types of amphibolites within the Qinling Group, north Qinling orogenic belt. Acta Petrologica Sinica 25, 2177–2194.
Yang, J., Gao, S., Chen, C., Tang, Y., Yuan, H., Gong, H., Xie, S., Wang, J., 2009. Episodic crustal growth of North China as revealed by U-Pb age and Hf isotopes of detrital zircons from modern rivers. Geochimica et Cosmochimica Acta 73, 2660–2673.
You, Z., Suo, S., Han, Y., Zhong, Z., Chen, N., 1991. The Metamorphic Progresses and Tectonic Analyses in the Core Complex of an Orogenic Belt: An Example from the Eastern Qinling Mountains. China University of Geosciences Press, Wuhan, 1–326.
You, Z.D., Han, Y.J., Suo, S.T., Chen, N.S., Zhong, Z.Q., 1993. Metamorphic history and tectonic evolution of the Qinling complex, eastern Qinling mountains, china. Journal of Metamorphic Geology 11, 549–560.
Yang, C., Zhang, S., Zhang, Z.Q., 1992. Features and significances of ancient shaping granite mass from Huxian County, Shaanxi. Bulletin of the Institute of Geology, Chinese Academy of Geological Sciences 25, 127–136.
Zhai, M.G., Santosh, M., 2011. The early Precambrian odyssey of the North China Craton: a synoptic overview. Gondwana Research 20, 6–25.
Zhai, M., Guo, J., Liu, W., 2005. Neoarchean to Paleoproterozoic continental evolution and tectonic history of the North China Craton: a review. Journal of Asian Earth Sciences 24, 547–561.
Zhang, B.R., Gao, S., Zhang, H.F., Han, Y.W., 2002. Geochemistry of the Qinling Orogenic Belt. Science Press, Beijing, 1–187.
Zhang, B.R., Zhang, H.F., Zhao, Z.D., Ling, W.L., 1996a. Geochemical subdivision and evolution of the lithosphere in east Qinling and adjacent regions – implications for tectonics. Science in China Series D-Earth Sciences 39, 245–255.
Zhang, C., Liu, L., Wang, T., Wang, X., Li, L., Gong, Q., Li, X., 2013. Granitic magmatism related to early Paleozoic continental collision in the North Qinling belt. Chinese Science Bulletin 58, 2323–2329.
Zhang, C., Liu, L., Zhang, G., Wang, T., Chen, D., Yuan, H., Liu, X., Yan, Y., 2004. Determination of Neoproterozoic post-collisional granites in the north Qinling Mountains and its tectonic significance. Earth Science Frontiers 11, 33–42.
Zhang, G., Zhang, B., Yuan, X., Xiao, Q., 2001. The Qinling Orogenic Belt and Continental Dynamics. Science Press, Beijing, 1–855.
Zhang, G.W., Meng, Q.G., Yu, Z.P., Sun, Y., Zhou, D.W., Guo, A.L., 1996b. Orogenesis and dynamics of the Qinling orogen. Science in China Series D-Earth Sciences 39, 225–234.
Zhang, J., Yu, S., Meng, F., 2011. Polyphase early Paleozoic metamorphism in the northern Qinling Orogenic Belt. Acta Petrologica Sinica 27, 1179–1190.
Zhang, Z., Liu, D., Fu, G., 1994. Study on the Isotopic Chronology of Metamorphic Strata in North Qinling. Geologicla Publishing house, Beijing, 1–191.
Zhang, Z., Zhang, Q., 1995. Geochemistry of metamorphosed late Proterozoic Kuanping ophiolite in the northern Qingling, China. Acta Petrologica Sinica 11 (Suppl.), 165–177.
Zhang, Z.Q., Zhang, G.W., Fu, G.M., Tang, S.H., Song, B., 1996c. Geochronology of metamorphic strata in the Qinling mountains and its tectonic implications. Science in China Series D-Earth Sciences 39, 283–292.
Zhao, G., Zhai, M., 2013. Lithotectonic elements of Precambrian basement in the North China Craton: review and tectonic implications. Gondwana Research 23, 1207–1240.
Zhu, X.Y., Chen, F., Li, S.Q., Yang, Y.Z., Nie, H., Siebel, W., Zhai, M.G., 2011. Crustal evolution of the North Qinling terrain of the Qinling Orogen, China: evidence from detrital zircon U-Pb ages and Hf isotopic composition. Gondwana Research 20, 194–204.